Atomic layer deposition of silicon nitride from bis(tertiary-butyl-amino)silane and N2 plasma studied by in situ gas phase and surface infrared spectroscopy

Please check the document version of this publication:

• A submitted manuscript is the version of the article upon submission and before peer-review. There can be important differences between the submitted version and the official published version of record. People interested in the research are advised to contact the author for the final version of the publication, or visit the DOI to the publisher's website.
• The final author version and the galley proof are versions of the publication after peer review.
• The final published version features the final layout of the paper including the volume, issue and page numbers.
Link to publication

Atomic Layer Deposition of Silicon Nitride from Bis(tertiary-butyl-amino)silane and N_2 Plasma Studied by *in Situ* Gas Phase and Surface Infrared Spectroscopy

Roger H. E. C. Bosch,[*,†] Lidewij E. Cornelissen,[†] Harm C. M. Knoops,[†,‡] and Wilhelmus M. M. Kessels[*,†]

[†]Eindhoven University of Technology, P.O. Box 513, 5600 MB Eindhoven, The Netherlands
[‡]Oxford Instruments Plasma Technology, North End, Bristol BS49 4AP, United Kingdom

Ⓢ *Supporting Information*

ABSTRACT: The atomic layer deposition process (ALD) of silicon nitride (SiN_x), employing bis(tertiary-butyl-amino)-silane ($SiH_2(NH^tBu)_2$, BTBAS) and N_2 plasma, was investigated by means of Fourier transform infrared (FT-IR) spectroscopy. *In situ* gas phase, film, and surface infrared measurements have been performed during different stages of the ALD process. From gas phase IR measurements it can be concluded that *tert*-butylamine is the main reaction product released during precursor exposure. Infrared measurements performed on the deposited SiN_x films revealed the incorporation of C in the form of CN and SiC, where more C is incorporated at a deposition temperature of 85 °C compared to 155 or 275 °C. Surface IR measurements, employing a four-axes sample manipulator, showed the formation of SiH- and NH-groups on the surface and revealed that most of the H is incorporated during the precursor exposure step. Furthermore, after the N_2 plasma step a vibrational mode around 2090 cm^{-1} was observed. This mode could be attributed to the formation of Si-NCH complexes and are likely to be formed by the so-called redeposition effect. For higher deposition temperatures, these Si-NCH complexes are removed again during the following precursor exposure step. At 85 °C, some of the complexes remain at the surface. Overall, from the gained knowledge about the surface chemistry, a reaction mechanism of the SiN_x ALD process has been proposed.
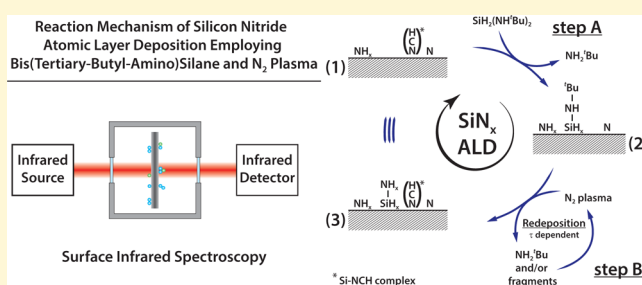
I. INTRODUCTION

In the past decade, the design of state-of-the-art field-effect transistors has changed substantially. Most prominently, new high-κ gate dielectrics have been introduced to replace the traditional SiO_2 gate dielectric, while metal gates replaced the polysilicon. Also the transistor lay-out changed from a planar structure to a 3D structure. The introduction of these new materials and transistor lay-outs introduced many technological challenges. For instance, thin-film materials are required to be deposited conformally, uniformly and with an excellent thickness control, while maintaining a high material quality. Atomic layer deposition (ALD) has become the method of choice to fulfill these requirements, and currently, ALD is applied in high-volume manufacturing for the preparation of high-κ metal gate stacks.[1]

An area in semiconductor manufacturing for which ALD is also gaining considerable interest, is in the field of gate spacer materials for transistor applications.[2−4] The deposition of such gate spacers becomes increasingly demanding, as the gate spacer should be conformally deposited over the sidewalls of the gate, while showing pitch independence, and, in many cases, takes place at a reduced thermal budget. At the same time the material should have a high wet-etch resistance, which sets strict demands on the atomic composition and the density of the

films. Silicon nitride (SiN_x) deposited by ALD is a suitable candidate to fulfill these requirements.

Several SiN_x ALD processes have been reported in the literature, where the majority of the processes use halide precursors, such as $SiCl_4$, SiH_2Cl_2, and Si_2Cl_6, at deposition temperatures above 400 °C.[5−11] During these processes hydrochloric acid is formed as byproduct. The hydrochloric acid formation and high temperature are undesired for certain applications of SiN_x spacers.[12] Therefore, low temperature ALD processes, using halide-free precursors, have been subject of investigation.[13−18] So far, these processes all use plasmas, as the high reactivity of the plasma species generally allow for the deposition of materials from a wider variety of precursors and at lower temperatures.[19]

One of the low temperature SiN_x processes recently reported in the literature employs bis(tertiary-butyl-amino)silane ($SiH_2(NH^tBu)_2$, BTBAS) as precursor and N_2 plasma as coreactant.[16] This process yields high quality SiN_x films with reasonably low impurity levels and that are fairly resistant against wet etching using a buffered HF solution.

A theoretical study, using density functional theory (DFT) calculations, has been performed by Ande et al. to determine the influence of the surface termination resulting from the N_2 plasma step on the growth of SiN_x using the aforementioned process.[20] Special interest was given to the experimental observation that the process works well with a N_2 plasma but has strongly reduced growth with NH_3, H_2, or N_2/H_2 plasmas. From the DFT calculations it was concluded that precursor adsorption requires undercoordinated bonds, which apparently can be generated sufficiently by a N_2 plasma and not with the other plasmas. H termination of the undercoordinated bonds is most probably the cause of the impeded growth when using NH_3, H_2, or N_2/H_2 plasmas.

Redeposition is another important effect that was identified to affect the SiN_x ALD process employing BTBAS and N_2 plasma.[17] The SiN_x process requires relatively long plasma exposures to minimize impurity levels and to obtain optimized material properties, such as the film density and wet-etch rate.[16] One role of the N_2 plasma is to remove the remaining precursor ligands, or fragments thereof, from the surface. Once liberated from the surface, these ligand species, which contain C and N, can be dissociated within the plasma, forming reactive species that can subsequently be redeposited on the surface. For short plasma exposures the redeposited species are likely to stay at the surface and get incorporated into the film. However, at extended N_2 plasma exposures, the redeposited species can be removed again. The species basically continuously undergo these redeposition−removal processes, while the reactor is being pumped and the reaction products are removed from the reactor over time. Therefore, the amount of redeposited species decreases with increasing plasma exposure time. Note that, by effectively reducing the gas residence time in the reactor, the effect of redeposition can be minimized.[17]

ALD is inherently governed by surface chemistry, and the aforementioned effects underline once more that the species present at the surface play a vital role. The surface species can impede the growth or can result in a SiN_x film with a low quality. Therefore, in this work we try to identify some elementary reactions that are taking place at the surface and we investigate the role of surface species during the SiN_x ALD process in greater detail. Insight into the species that are present at the surface during different stages of the ALD process has been obtained by a combination of in situ gas phase and surface infrared measurements. The measurements give information about how the precursor molecules and N_2 plasma react with the surface and what the main reaction products are of both half-cycles. The work has resulted into a better understanding of the surface chemistry of the SiN_x ALD process and enabled us to postulate a reaction mechanism of the SiN_x process investigated.

II. EXPERIMENTAL DETAILS

The SiN_x ALD experiments were carried out in a home-built plasma-assisted ALD reactor. A schematic representation of the setup is shown in Figure 1. This figure also shows the diagnostic techniques used in this work as well as a drawing of the BTBAS molecule.

The reactor was equipped with an inductively coupled plasma (ICP) source consisting of a quartz tube, Cu coil, and power supply with an automated matching network. The plasma source was operated at a power of 100 W and frequency of 13.56 MHz. During the 10 s N_2 plasma exposure, the pressure in the reactor was regulated to 1.5×10^{-2} mbar. The BTBAS precursor (Air Products Inc., purity ≥ 98.5%) was kept in a stainless steel bubbler at a temperature of 50 °C and was vapor drawn into the reactor chamber via stainless steel
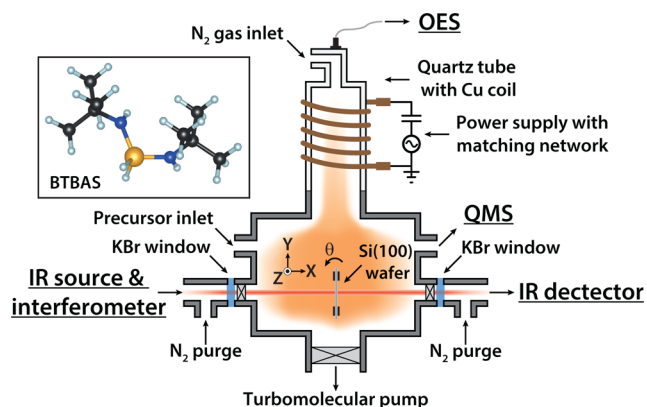
Figure 1. Schematic representation of the ALD setup, including the optical emission spectroscopy (OES), quadrupole mass spectrometry (QMS), and infrared (IR) spectroscopic techniques. The inset shows a drawing of the BTBAS precursor molecule.

tubing, which was heated to 70 °C. The reactor wall was heated to 100 °C. During the precursor half-cycle the valve between the reaction chamber and the turbomolecular pump was closed. This was done to increase the precursor reaction time and minimize precursor consumption. The BTBAS dose itself was 150 ms, while the bottom valve of the reactor was closed for 4 s. Sufficiently long pump and purge steps (>2 s) were applied in between the ALD half-cycles to remove the reaction products and the excess amount of precursor or coreactant from the reactor.

A ~500 μm thick Si(100) double-side polished wafer (n-type doping, 30−50 Ω·cm) with native oxide was used as substrate. The substrate was mounted onto a sample manipulator (PREVAC, four-axes manipulator), which enabled for a well-controlled movement of the sample in the X, Y, and Z directions as defined in Figure 1. The sample could also be rotated around the Z-axis between $-90° < \theta < 90°$, where $\theta = 0°$ is defined as the sample being in the vertical position, i.e., surface normal of the sample was parallel to the X-axis. Note that the substrate mounting differs significantly from our previously reported FT-IR study on a three-step room temperature Pt ALD process.[21] The sample was resistively heated between 85 and 275 °C by applying an AC current through the Si(100) wafer. Since the resistance of Si decreases rapidly with increasing temperatures, i.e., Si acts as NTC thermistor, two 100 W halogen light bulbs were added to electrical circuit in series. These light bulbs act as PTC thermistors and limit the current when the resistance of the wafer drops. In addition, the temperature was regulated using a EuroTherm temperature controller (type 2132) combined with a K-type thermocouple fixed to the substrate using conductive silver paste.

The infrared setup consisted of a Bruker Vector 22 Fourier-transform infrared (FT-IR) spectrometer with a mid-infrared light source (Globar ~10,000 to 50 cm^{-1}). The Si(100) substrate was placed vertically into the IR beam, i.e., $\theta = 0°$. The SiN_x film was symmetrically deposited on both sides of the Si(100) wafer. The intensity of the transmitted IR light was measured using a liquid N_2 cooled mercury cadmium tellurium (MCT) detector (Bruker D316) with a spectral range of 12,000 to 550 cm^{-1}. The Vector 22 as well as the environment of the MCT detector were purged with dry N_2 gas. KBr windows were used as entry and exit windows for the IR light. In order to prevent deposition on these windows, gate valves were installed and only opened during the actual IR measurements. The infrared absorbances were calculated by $A = -^{10}\log\left(\frac{I}{I_0}\right)$, with I and I_0 the measured intensity of the sample and reference, respectively. Each presented absorbance spectrum is a result of an average of multiple intensity measurements to achieve a high signal-to-noise ratio, where each intensity measurement typically consisted of 1024 scans.

Optical emission spectroscopy (OES) measurements were carried out using an Ocean Optics USB4000-UV-VIS spectrometer. This spectrometer has a wavelength detection range of 200−1100 nm and a

resolution of ∼1 nm. The optical fiber was placed at the top of the quartz tube of the plasma source, see Figure 1. This configuration resulted in a line-of-sight measurement through the plasma source into the deposition chamber.

For film characterization, Rutherford backscattering spectrometry (RBS) and elastic recoil detection (ERD) measurements have been performed by the company AccTecc BV (Eindhoven). A high energy (1.8−2 MeV) beam of He ions was used to probe the sample and to determine the elemental composition of the SiN_x films. The areal film densities of the elements have been used to calculate atomic percentages (at. %) and the number of Si atoms deposited per ALD cycle per unit area (at./nm^2). Film growth was also monitored by *in situ* spectroscopic ellipsometry (SE) using a J. A. Woollam, Inc. M2000U visible ellipsometer (1.2−5.0 eV) at an angle of incidence of 68°. The sample was rotated 90° in this case. The dielectric constants and thickness of the SiN_x films were extracted from the SE data using a Tauc−Lorentz model.[22]

III. SIN$_X$ FILM COMPOSITION

First the film properties of the deposited SiN_x films have been investigated, as the SiN_x process was newly introduced on the home-built ALD reactor. In our previous work, the SiN_x films were deposited on a Oxford Instruments FlexAl reactor.[16,17] SE, RBS, and ERD have been applied to determine the refractive index, growth per cycle (GPC), N/Si ratio, and the C, O, and H concentration in the films. Table 1 gives an overview of the

**Table 1. Material Properties of the SiN_x Films Deposited within This Work as a Function of the Sample Temperature**[a]

T_{sample} (°C)	n (@ 2 eV)	GPC (Å)	GPC (Si atoms/ nm^2)	N/ Si	[C] (at. %)	[O] (at. %)	[H] (at. %)
85	1.69	0.8	1.2				
155	1.88	0.3	0.9	1.4	8	9	10
275	1.94	0.2	0.8	1.4	3	9	7

[a]Properties have been determined using SE, RBS, and ERD.

results. The GPC, C content, and H content all increase with decreasing temperature. Despite that more Si atoms are deposited per cycle at lower temperatures, the N/Si ratio appears unaffected by the temperature between 155 and 275 °C. The films deposited at 85 °C oxidize completely after exposure to the ambient; henceforth, the N/Si, [C], [O], and [H] could not be determined reliably by RBS and ERD for this sample. It can, however, be expected that the [C] and [H] density increase even further when depositing at 85 °C.

In situ IR measurements have been performed on the SiN_x films to investigate the film composition in more detail. These measurements give insight into how the elements present in the SiN_x film are chemically bonded. Figure 2 shows the *in situ* IR spectra of SiN_x films deposited at 85, 155, and 275 °C. The reference spectrum (I_0) was measured before the depositions, i.e., for a clean Si(100) substrate, while the measurement I was measured after the ALD cycles. As the samples were kept in vacuum and not exposed to the ambient, postdeposition oxidization was prevented. The absorbances have been scaled to the number of ALD cycles, which allows for an easy comparison of the spectra.

The spectra of Figure 2 show several spectral features that depend on the sample temperature: (1) The peak between 670 and 1100 cm^{-1} is related to Si−N stretch modes in the SiN_x film.[23−25] For lower temperatures one of the Si−N stretching modes becomes more dominant as indicated by the vibrational mode at 935 cm^{-1} in Figure 2a. This is most probably caused
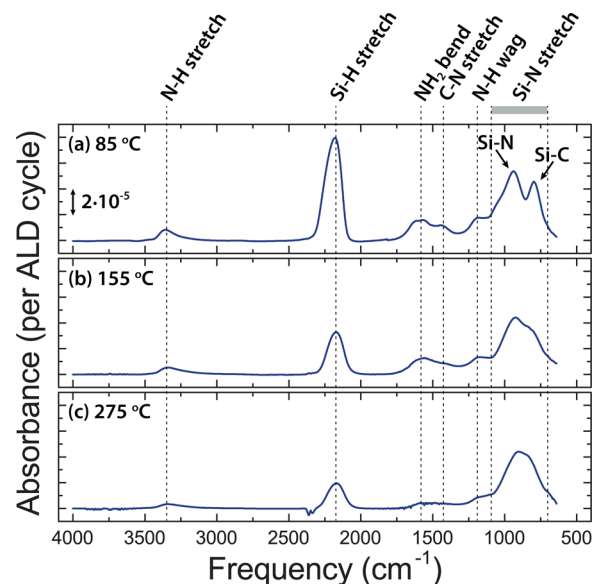
Figure 2. Absorbance spectra of SiN_x films deposited at (a) 85, (b) 155, and (c) 275 °C. The spectra reveal information on the film composition and bondings through the peaks assigned. The spectra have been scaled to the number of ALD cycles such that the absorbance is given per ALD cycle. The scale is equal for all three graphs.

by the increase in hydrogen incorporation for lower temperatures, as Lucovsky et al. suggest that the Si−N frequency shifts to higher values as neighboring Si atoms are replaced by H.[23] (2) At ∼800 cm^{-1} a peak is visible at a deposition temperature of 85 °C, while this peak is absent for the 275 °C. This feature can be attributed to Si−C bonds.[26,27] In addition, the peak at 1430 cm^{-1} is related to C−N stretch.[28] Both the Si−C and C−N stretch vibrational modes indicate that more carbon is incorporated into the SiN_x film as the deposition temperature is decreased. This claim is supported by the RBS results in Table 1. (3) Hydrogen is incorporated into the films in the form of NH_x and SiH_x as indicated by the resonances at 1180, 1560, 2175, and 3360 cm^{-1}.[29] The resonance at 1560 cm^{-1} indicates the presence of NH_2. All these H-related vibrational modes increase with decreasing temperature, i.e., more H incorporation at lower temperatures. This is also in agreement with the ERD data in Table 1. Altogether, the trends obtained for ALD of SiN_x in the home-built reactor are similar to those observed in our previous work for ALD of SiN_x on a Oxford Instruments FlexAL reactor.[16]

IV. SIN$_X$ GROWTH

To obtain insight into the surface reactions during SiN_x ALD, the half-cycles of the SiN_x ALD process have been studied by *in situ* gas phase and surface IR spectroscopy. These studies have been complemented with OES and QMS measurements. From the combination of these measurements it can be determined which species are present in the gas phase (Section A) and at the surface (Section B) during different stages of the ALD process. Also the influence of the sample temperature has been investigated (Section C).

A. Gas Phase Species. By closing the valve between the reactor vessel and the turbomolecular pump (see Figure 1), it is possible to confine molecules in the reactor and perform gas phase IR measurements on these molecules. When BTBAS molecules are introduced into the reactor, they react with

available reactive sites at the sample and reactor wall while liberating certain reaction products. Figure 3a shows a gas
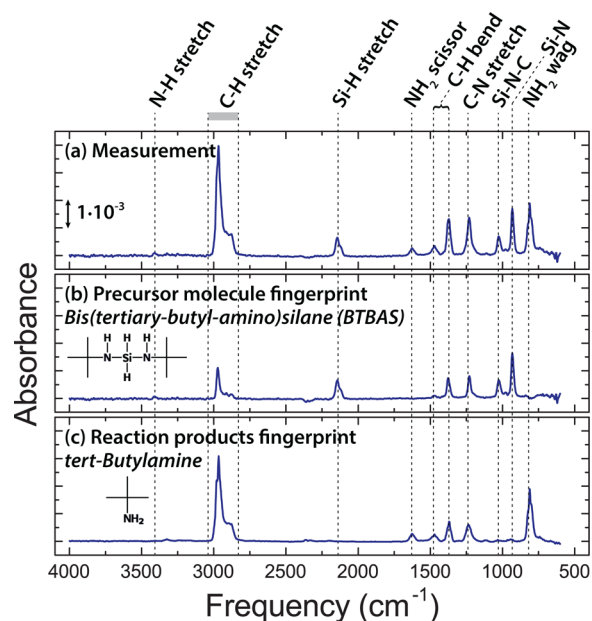
Figure 3. (a) Gas phase IR spectrum of the species present during the precursor step for ALD of SiN_x. (b) Vibrational fingerprint of the BTBAS molecule. (c) Vibrational fingerprint of the reaction product, which has been identified as *tert*-butylamine. The vibrational modes have been assigned as indicated. The scale is equal for all three graphs.

phase infrared measurement, performed at 85 °C, after a high BTBAS dose, i.e., a dose leading to full saturation of the surface reactions. The absorbance has been calculated by measuring the IR intensity before and after the precursor dose, resulting in I_0 and I, respectively. Hence, this absorbance spectrum contains information about the precursor as well as the reaction products. By performing an additional measurement with an unsaturated BTBAS dose it is possible to identify the so-called vibrational fingerprints of the precursor and reaction products, Figure 3b,c, respectively. Both fingerprints show vibrational modes present at 1370, 1480, and 2875−2975 cm^{-1}. These peaks can be attributed to the C−H bending and stretching modes, respectively.[28] The vibrational modes at 1250 cm^{-1} in both fingerprints are related to C−N stretch.[30] In the fingerprint of the precursor molecule, as shown in Figure 3b, the Si−H stretching mode around 2144 cm^{-1} is visible, as well as the Si−N−C stretching mode at 1025 cm^{-1} and the Si−N stretching mode at 931 cm^{-1}.[28,30] These three modes are very characteristic for the precursor molecule. In addition to these modes, a small peak is visible at 3410 cm^{-1}, which is related to N−H stretch.[30] The vibrational fingerprint of the reaction products, as shown in Figure 3c, corresponds to the spectrum of *tert*-butylamine as can be found in the NIST database.[31] This spectrum contains NH_2 scissoring and wagging modes at 1629 and 810 cm^{-1}, respectively.[30] Both modes are characteristic for the reaction products, as no NH_2 group is present in the precursor molecule. The formation of *tert*-butylamine as the main reaction product indicates that the Si−N bond in the precursor molecule breaks during the reaction with the surface, while the ligand picks up an additional H atom. It also suggests that the ligand itself stays intact during the precursor exposure, meaning only the Si−N bond breaks while the other bonds remain unaffected.

Gas phase IR measurements of the plasma half-cycle were not possible, as the gas phase species could not be confined in the reactor vessel by closing the bottom valve while igniting a plasma without affecting the plasma properties significantly. Therefore, the gas phase species present in the reactor during the N_2 plasma step were studied using optical emission spectroscopy (OES) and quadrupole mass spectrometry (QMS). The measurements were performed in a reactor with a similar design (Oxford Instruments FlexAL).[16,17] Figure 4
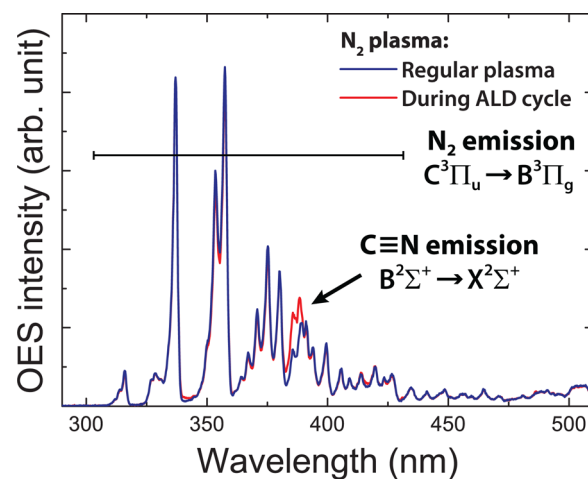
Figure 4. Optical emission data of a regular N_2 plasma and during an ALD cycle. For both spectra, N_2 emission from the $C^3\Pi_u \rightarrow B^3\Pi_g$ transition is present in this wavelength range. However, during the ALD cycle an increased signal at 388 nm is present due to additional C≡N emission, originating from the $B^2\Sigma^+ \rightarrow X^2\Sigma^+$ transition of the C≡N violet system.

shows the data of two OES measurements. One was measured during a regular N_2 plasma, while the other was measured during a SiN_x ALD cycle. When comparing the two spectra, an increased signal was present at ∼388 nm during the ALD cycle. This increased signal corresponds to C≡N emission, originating from the $B^2\Sigma^+ \rightarrow X^2\Sigma^+$ transition of the C≡N violet system.[32,33] Furthermore, the QMS data indicates, among others, the presence of *tert*-butylamine, cyanogen (C_2N_2), hydrogen cyanide (HCN), and ammonia (NH_3) during the N_2 plasma step, as can be seen in Figure S1 of the Supporting Information. The presence of *tert*-butylamine suggests that a part of the adsorbed precursor ligands are only liberated during the N_2 plasma step while also staying intact, i.e., did not break into smaller fragments either during the precursor adsorption step or the plasma step. Nonetheless, the presence of the C_2N_2, HCN, and NH_3 demonstrates that some ligands do fragment during the precursor adsorption or the N_2 plasma step. This includes the dissociation of reaction products in the plasma itself. In either case, some of these fragments can redeposit on the surface as they are reactive species.

B. Surface Species. The species present at the surface during the SiN_x ALD process have been measured by surface IR spectroscopy. Figure 5 shows the data for a SiN_x sample, which has been deposited at a temperature of 155 °C. Figure 5b shows the spectra corresponding to the two individual half-cycles. The absorbance spectra have been determined by measuring the IR intensity spectrum I after the half-cycle, i.e., after the precursor dose or the N_2 plasma step, while the reference intensity spectrum I_0 was measured before the half-
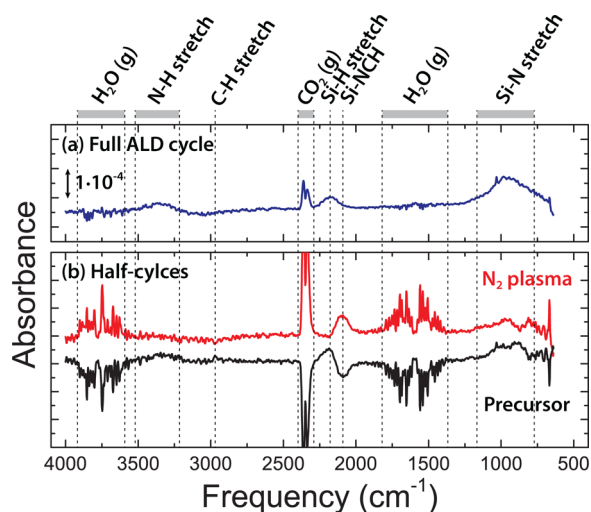
Figure 5. (a) Surface IR spectrum of a full ALD cycle of SiN_x. (b) Surface IR spectra of the BTBAS precursor and N_2 plasma half-cycle. All measurements were done at a deposition temperature of 155 °C. The vibrational modes have been assigned as indicated, where the modes related to $H_2O(g)$ and $CO_2(g)$ originate from remaining gas species present in the reactor as well as from fluctuations in the N_2-purged IR beam path. The scale is equal for both graphs.

cycle. The positive and negative peaks, with respect to the baseline, correspond to the species that are created at and removed from the surface during a half-cycle, respectively. Note that this does not hold for the modes related to $H_2O(g)$ and $CO_2(g)$, as those peaks originate from remaining gas species present in the reactor as well as from fluctuations in the N_2-purged IR beam path. At the surface, the formation of Si−N bonds is observed during both half-cycles, as indicated by the Si−N stretching modes between 760 and 1200 cm^{-1}.[23−25] The modes at ∼2180 cm^{-1} and in the region 3200−3510 cm^{-1} are related to the stretching modes of Si−H and N−H, respectively.[29,30] The majority of the N−H and Si−H is incorporated during the precursor half-cycle, as these modes are nearly absent in the spectrum of the N_2 plasma half-cycle. The summation of the two half-cycle absorbance spectra results in the spectrum of the full ALD cycle, as shown in Figure 5a. The modes in this graph correspond to the species that have been incorporated into the SiN_x film after one complete cycle of ALD. The figure shows the incorporation of SiH and NH groups.

At two distinct frequencies, species are observed that are formed in one-half-cycle and removed in the other one: (1) At ∼2970 cm^{-1} some small traces of C−H stretch are visible in spectrum of the precursor half-cycle, which indicate that CH species are present at the surface after the precursor dose.[28] The CH species are removed again during the N_2 plasma exposure. The vibrational modes are barely visible and almost at the noise level even with a lot of averaging. However, the signal is consistently observed throughout many experiments as also will be shown in Section C. These CH species are likely related to precursor ligands, or fragments thereof, that remain at the surface after precursor exposure. (2) At ∼2090 cm^{-1} a vibrational mode is present that is formed during the N_2 plasma step and removed during the following precursor step. The assignment of this mode is not straightforward, but after careful consideration, it has been concluded that it cannot be attributed to Si−H vibrational modes, as the frequency does not match with the expected bonding configuration. It should

also be noted that the removal of the mode does not necessarily indicate that the associated surface species is removed from the surface. It can also remain at the surface but become IR inactive due to a change in bonding configuration. On the basis of literature reports, the origin of this vibrational mode has been attributed to the formation of a Si−NCH complex at the surface.[34−38] Laidig et al. showed that the vibrational frequency of HCN is ∼2130 cm^{-1}, while for HNC it is 2061−2067 cm^{-1}.[34] Bu et al. describe the interaction of HCN with a Si covered surface.[35,36] They show the formation of −C≡N at a frequency of ∼2056 cm^{-1}, while Tiznado et al. assigns this peak to −N≡C.[38] Hence, the exact bonding configuration of the Si−NCH complex within this work is unclear, i.e., unclear if H is attached to C or N and if a Si−N or Si−C bond is formed. A possible origin of this Si−NCH complex is redeposition of precursor fragments. During the N_2 plasma step, C≡N emission and the formation of HCN have been observed by OES and QMS, as discussed in the previous section. These species could react with the surface, forming the Si−NCH complex. In the next half-cycle, the precursor exposure removes the complex or alters it chemically, such that it disappears from the IR spectrum.

C. Temperature Dependence. The substrate temperature plays an important role in many ALD processes. This is also the case for the SiN_x process, as relatively large changes in material composition have been observed as a function of the substrate temperature. Table 1 illustrated that the growth per cycle increases for decreasing sample temperatures and that the amount of carbon present in the film goes up as well. In this section, the temperature dependence of the SiN_x process in discussed in more detail, as IR surface measurements have been performed at 85, 155, and 275 °C.

Strikingly, the absorbance spectra corresponding to the half-cycles did not show a strong dependence on the deposition temperature for the temperature range studied within this work. The spectra at 85 and 275 °C looked quite similar to those of 155 °C in Figure 5. This suggests that the surface chemistry does not change much with substrate temperature. However, in two regions the vibrational modes do show a temperature dependence. First, Figure 6 shows the half-cycle IR spectra for the three different deposition temperatures in the frequency range between 2750 and 3250 cm^{-1}. This range is characteristic for CH groups present at the surface. For the deposition temperatures of 85 and 155 °C, CH groups can be clearly observed from the modes at ∼2970 cm^{-1}. These groups are formed during the precursor half-cycle and removed during the N_2 plasma exposure. At 275 °C, a peak at this position cannot be distinguished from the noise. This suggests that less CH groups are present at the surface at higher temperatures after the precursor step. Note that the growth per cycle is also lower for higher deposition temperatures, which indicates less precursor adsorption and hence a lower CH coverage. Furthermore, CH groups could desorb from the surface during the IR measurement, as it takes considerable time (∼30 min for the I and I_0 measurement each) to collect sufficient scans to determine the absorbance of a half-cycle with a reliable signal-to-noise ratio.

The second region where the absorbance varies with the deposition temperature is between 1950 and 2450 cm^{-1}, as is shown in Figure 7. In this region the formation of Si−H can be observed at ∼2180 cm^{-1} as well as the formation and disappearance of the alleged Si−NCH complex between 2080 and 2110 cm^{-1}. At 85 °C there is more Si−H incorporation
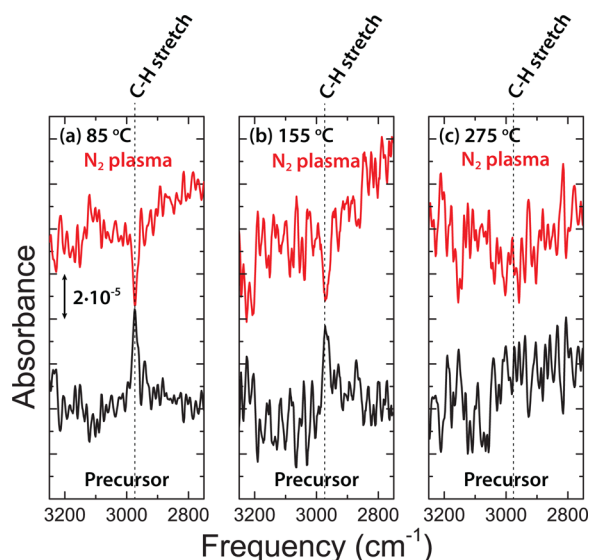
Figure 6. Surface IR spectra as a function of the deposition temperature; (a) 85, (b) 155, and (c) 275 °C. In the frequency range between 2750 and 3250 cm^{-1}, the C−H stretch modes are present, as indicated. The scale is equal for all three graphs.
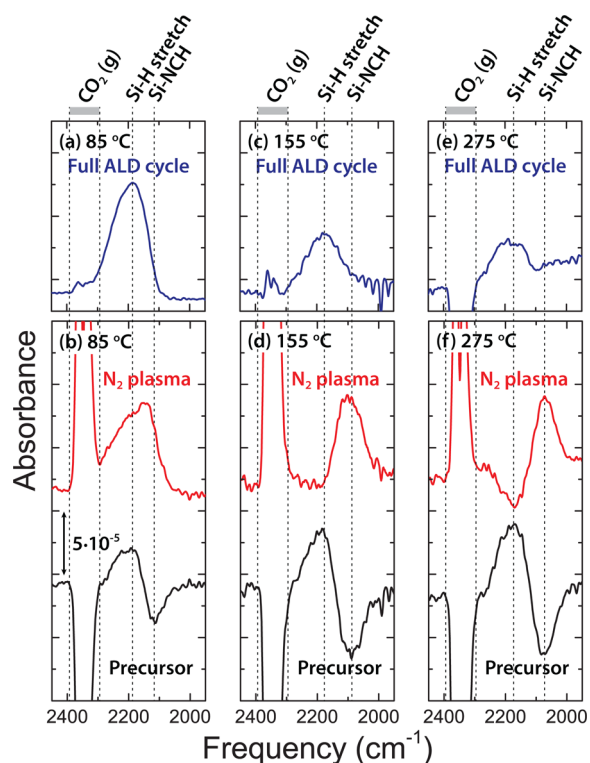

Figure 7. Surface IR spectra of the full ALD cycle (a,c,e) and the individual half-cycles (b,d,f), all as a function of the deposition temperature; (a,b) 85, (c,d) 155, and (e,f) 275 °C. In the frequency range between 1950 and 2450 cm^{-1}, the Si−H stretch and Si−NCH modes are present, as indicated. The modes related to CO_2(g) originate from remaining gas species present in the reactor. The scale is equal for all graphs.

compared to 155 and 275 °C, as can be seen in the full ALD cycle spectra of Figure 7a,c,e, respectively. Moreover, during the N_2 plasma step at 275 °C, shown in Figure 7f, some Si−H appears to have even been removed. The removal of Si−H could also explain why less H is incorporated at higher

temperatures, as depicted by the H content given in Table 1. Table 1 as well as Figure 2 also showed more C incorporation for lower deposition temperatures. This could be linked to less removal of the Si−NCH complex during the precursor step at lower temperatures. After the N_2 plasma, the magnitude of the Si−NCH vibrational modes, as shown in Figure 7b,d,f, is similar. However, after the precursor half-cycle, the mode at ∼2110 cm^{-1} in Figure 7b seems smaller, i.e., less removed, than the one at ∼2090 and ∼2080 cm^{-1} for 155 and 275 °C (Figures 7d,f, respectively). Due to red-shift of the Si−NCH peak with decreasing temperatures and the overlap with the Si−H peak, it is hard to determine the magnitude of each vibrational mode reliably. Nonetheless, the observed differences suggest less removal of Si−NCH at lower temperatures, which results in more C incorporation at lower deposition temperatures.

V. DISCUSSION

In this work, the surface chemistry of the SiN_x ALD process employing BTBAS and N_2 plasma was investigated. The presented IR measurements, complemented with the RBS, ERD, OES, and QMS data, can be combined to propose a reaction mechanism. This proposed mechanism is schematically shown in Figure 8.
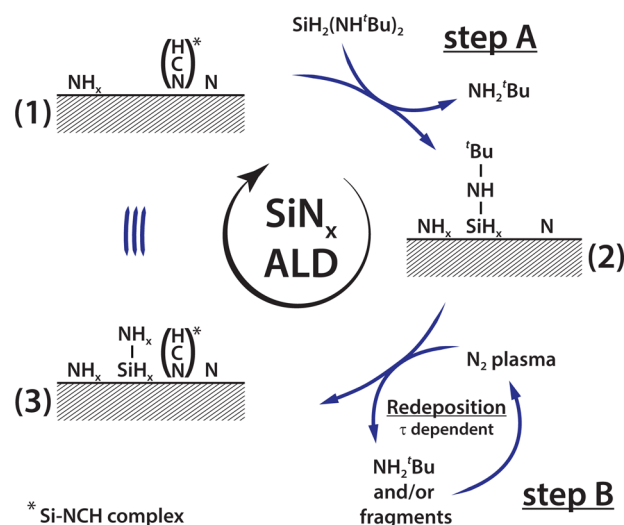
Figure 8. Schematic representation of the proposed reaction mechanism for SiN_x ALD employing BTBAS (step A) and N_2 plasma (step B). (1) The surface before precursor exposure highlighting several surface groups that can be present. (2) The surface after the precursor exposure, where NH_2^tBu is liberated as main reaction product. The effect of redeposition has been indicated in step B, where the NH_2^tBu and/or fragments liberated by the N_2 plasma also act as feedstock species. The effect of redeposition depends on the gas residence time (τ). (3) The surface after the N_2 plasma, where a Si−NCH complex has been formed at the surface. More details of this proposed reaction mechanism are given in the text.

Figure 8 illustrates the important features of the SiN_x process, where several species present at the surface during different stages of the SiN_x ALD cycle have been highlighted. In situation (1), the surface before the precursor exposure is shown. The surface contains NH_x groups and Si−NCH complexes formed in the previous ALD cycle. When the BTBAS precursor is introduced in step A, the precursor molecule reacts with the surface and part of the ligands are liberated as *tert*-butylamine. The remaining ligands stay at the

surface as depicted in situation (2). During the N_2 plasma, the remaining precursor ligands, or fragments thereof, are removed and enter the plasma. These removed species can dissociate within the plasma and redeposit on the surface. Due to this effect of redeposition, Si−NCH complexes are formed at the surface as shown in situation (3). This surface is identical to the one of situation (1), but with some additional SiN_x deposited.

In step A the BTBAS precursor is introduced into the reactor. The precursor molecule contains two amine ligands (NH^{t}Bu), of which some are liberated as *tert*-butylamine during the precursor exposure. This claim is supported by the gas phase IR measurements, as *tert*-butylamine molecules have been observed during the precursor exposure. Furthermore, some of the ligands, or fragments thereof, stay attached to the surface, as *tert*-butylamine is also measured by QMS during the N_2 plasma exposure in the second half-cycle. It is unclear at this moment if, on average, one ligand per adsorbed precursor molecule is removed during the precursor half-cycle, or less or more than one *tert*-butylamine ligand. For simplicity, the liberation of one amino ligand per adsorbed precursor molecule is assumed in Figure 8.

During the N_2 plasma in step B, the OES measurements showed the presence of excited CN species within the plasma, and QMS indicated, among others, the presence of HCN. In addition, the surface infrared measurements revealed the formation of a Si−NCH complex at the surface. A possible origin of this complex is the presence of HCN, or related species, within the N_2 plasma which (re)deposit on the surface, similar to the process described by Bacalzo-Gladden et al.[39] In their computational study they show that HCN can readily adsorb on a Si(100) surface. The Si−NCH is removed, or its bonding configuration becomes IR inactive, during the precursor step, as is indicated by the peaks between 2080 and 2110 cm^{-1} in the precursor spectra of Figures 5 and 7. However, the exact mechanism is unclear at this stage. At low deposition temperatures, inefficient removal of this Si−NCH complex is observed and is most probably responsible for the larger C incorporation. This is likely because the carbon contamination is incorporated as Si−C and C−N, as shown by the film IR measurements in Figure 2.

VI. CONCLUSION

The atomic layer deposition process of SiN_x, employing BTBAS and N_2 plasma, was studied by FT-IR spectroscopy. Gas phase as well as surface IR measurements were carried out to probe reaction products and surface groups during both half-cycles in order to gain a better understanding of the surface chemistry. On the basis of the data, we have proposed a reaction mechanism with the following important aspects: (1) when the BTBAS precursor molecule reacts with the surface, *tert*-butylamine is liberated as the main reaction product. Some of the ligands, or fragments thereof, stay at the surface and are only removed during the N_2 plasma in the next half-cycle. (2) Hydrogen in the SiN_x film originates mainly from the precursor molecule and is primarily bonded to Si. For lower deposition temperature the H incorporation increases. (3) During the N_2 plasma step, the formation of Si-NCH complexes at the surface has been observed. These complexes remain at the surface but are removed during the precursor exposure. This removal seems temperature dependent, i.e., less removal for lower deposition temperatures. This coincides with the fact that more SiC and CN are incorporated into the film at lower deposition temperatures. The origin of the Si−NCH complex is likely to be related to the effect of redeposition, where species that are removed from the surface can redeposit on the surface during the N_2 plasma exposure.

ASSOCIATED CONTENT

Ⓢ Supporting Information

The Supporting Information is available free of charge on the ACS Publications website at DOI: 10.1021/acs.chemmater.6b02319.

Description of the quadrupole mass spectrometry (QMS) experimental setup, performed measurements, and data analysis; determined mass spectra of the reaction products, including comparison with spectra found in the NIST database; conclusion of which species are likely to be present in the reactor during the N_2 plasma step (PDF)

AUTHOR INFORMATION

Corresponding Authors
*E-mail: r.h.e.c.bosch@tue.nl.
*E-mail: w.m.m.kessels@tue.nl.

Notes
The authors declare no competing financial interest.

ACKNOWLEDGMENTS

REFERENCES

(1) Johnson, R. W.; Hultqvist, A.; Bent, S. F. A Brief Review of Atomic Layer Deposition: From Fundamentals to Applications. *Mater. Today* **2014**, *17*, 236−246.

(2) Ga-Won, L.; Hi-Duck, L.; Kwan-Yong, L.; Yong Soo, K.; Hong-Sun, Y.; Gyu-Seog, C.; Sung-Kye, P.; Sung-Joo, H. Characterization of Polymetal Gate Transistors with Low-Temperature Atomic-Layer-Deposition-Grown Oxide Spacer. *IEEE Electron Device Lett.* **2009**, *30*, 181−184.

(3) Endo, K.; Ishikawa, Y.; Matsukawa, T.; Liu, Y.; O'uchi, S.-I.; Sakamoto, K.; Tsukada, J.; Yamauchi, H.; Masahara, M. Enhancement of FinFET Performance Using 25-nm-thin Sidewall Spacer Grown by Atomic Layer Deposition. *Solid-State Electron.* **2012**, *74*, 13−18.

(4) Koehler, F.; Triyoso, D. H.; Hussain, I.; Mutas, S.; Bernhardt, H. Atomic Layer Deposition of SiN for Spacer Applications in High-End Logic Devices. *IOP Conf. Ser.: Mater. Sci. Eng.* **2012**, *41*, 012006.

(5) Goto, H.; Shibahara, K.; Yokoyama, S. Atomic Layer Controlled Deposition of Silicon Nitride With Self-Limiting Mechanism. *Appl. Phys. Lett.* **1996**, *68*, 3257−3259.

(6) Yokoyama, S.; Goto, H.; Miyamoto, T.; Ikeda, N.; Shibahara, K. Atomic Layer Controlled Deposition of Silicon Nitride and in situ Growth Observation by Infrared Reflection Absorption Spectroscopy. *Appl. Surf. Sci.* **1997**, *112*, 75−81.

(7) Morishita, S.; Sugahara, S.; Matsumura, M. Atomic-Layer Chemical-Vapor-Deposition of Silicon-Nitride. *Appl. Surf. Sci.* **1997**, *112*, 198−204.

(8) Klaus, J. W.; Ott, A. W.; Dillon, A. C.; George, S. M. Atomic Layer Controlled Growth of Si3N4 Films Using Sequential Surface Reactions. *Surf. Sci.* **1998**, *418*, L14−L19.

(9) Nakajima, A.; Khosru, Q. D. M.; Yoshimoto, T.; Kidera, T.; Yokoyama, S. NH3-Annealed Atomic-Layer-Deposited Silicon Nitride As a High-K Gate Dielectric with High Reliability. *Appl. Phys. Lett.* **2002**, *80*, 1252−1254.

(10) Park, K.; Yun, W.-D.; Choi, B.-J.; Kim, H.-D.; Lee, W.-J.; Rha, S.-K.; Park, C. O. Growth Studies and Characterization of Silicon Nitride Thin Films Deposited by Alternating Exposures to Si_2Cl_6 and NH_3. *Thin Solid Films* **2009**, *517*, 3975−3978.

(11) Ovanesyan, R. A.; Hausmann, D. M.; Agarwal, S. Low-Temperature Conformal Atomic Layer Deposition of SiN_x Films Using Si_2Cl_6 and NH_3 Plasma. *ACS Appl. Mater. Interfaces* **2015**, *7*, 10806−10813.

(12) Koehler, F.; Triyoso, D. H.; Hussain, I.; Antonioli, B.; Hempel, K. Challenges in Spacer Process Development for Leading-Edge High-K Metal Gate Technology. *Phys. status solidi* **2014**, *11*, 73−76.

(13) King, S. W. Plasma Enhanced Atomic Layer Deposition of SiN_x:H and SiO_2. *J. Vac. Sci. Technol., A* **2011**, *29*, 041501.

(14) Triyoso, D. H.; Hempel, K.; Ohsiek, S.; Jaschke, V.; Shu, J.; Mutas, S.; Dittmar, K.; Schaeffer, J.; Utess, D.; Lenski, M. Evaluation of Low Temperature Silicon Nitride Spacer for High-K Metal Gate Integration. *ECS J. Solid State Sci. Technol.* **2013**, *2*, N222−N227.

(15) Jang, W.; Jeon, H.; Kang, C.; Song, H.; Park, J.; Kim, H.; Seo, H.; Leskela, M.; Jeon, H. Temperature Dependence of Silicon Nitride Deposited by Remote Plasma Atomic Layer Deposition. *Phys. Status Solidi A* **2014**, *211*, 2166−2171.

(16) Knoops, H. C. M.; Braeken, E. M. J.; de Peuter, K.; Potts, S. E.; Haukka, S.; Pore, V.; Kessels, W. M. M. Atomic Layer Deposition of Silicon Nitride from Bis(Tert-Butylamino)Silane and N_2 Plasma. *ACS Appl. Mater. Interfaces* **2015**, *7*, 19857−19862.

(17) Knoops, H. C. M.; de Peuter, K.; Kessels, W. M. M. Redeposition in Plasma-Assisted Atomic Layer Deposition: Silicon Nitride Film Quality Ruled by the Gas Residence Time. *Appl. Phys. Lett.* **2015**, *107*, 014102.

(18) Weeks, S.; Nowling, G.; Fuchigami, N.; Bowes, M.; Littau, K. Plasma Enhanced Atomic Layer Deposition of Silicon Nitride Using Neopentasilane. *J. Vac. Sci. Technol., A* **2016**, *34*, 01A140.

(19) Profijt, H. B.; Potts, S. E.; van de Sanden, M. C. M.; Kessels, W. M. M. Plasma-Assisted Atomic Layer Deposition: Basics, Opportunities, and Challenges. *J. Vac. Sci. Technol., A* **2011**, *29*, 050801.

(20) Ande, C. K.; Knoops, H. C. M.; de Peuter, K.; van Drunen, M.; Elliott, S. D.; Kessels, W. M. M. Role of Surface Termination in Atomic Layer Deposition of Silicon Nitride. *J. Phys. Chem. Lett.* **2015**, *6*, 3610−3614.

(21) Bosch, R. H. E. C.; Bloksma, F. L.; Huijs, J. M. M.; Verheijen, M. A.; Kessels, W. M. M. Surface Infrared Spectroscopy during Low Temperature Growth of Supported Pt Nanoparticles by Atomic Layer Deposition. *J. Phys. Chem. C* **2016**, *120*, 750−755.

(22) Jellison, G. E.; Modine, F. A. Parameterization of the Optical Functions of Amorphous Materials in the Interband Region. *Appl. Phys. Lett.* **1996**, *69*, 371−373.

(23) Lucovsky, G.; Yang, J.; Chao, S.; Tyler, J.; Czubatyj, W. Nitrogen-Bonding Environments in Glow-Discharge-Deposited a-Si:H Films. *Phys. Rev. B: Condens. Matter Mater. Phys.* **1983**, *28*, 3234−3240.

(24) Tsu, D. V.; Lucovsky, G.; Mantini, M. J. Local Atomic Structure in Thin Films of Silicon Nitride and Silicon Diimide Produced by Remote Plasma-Enhanced Chemical-Vapor Deposition. *Phys. Rev. B: Condens. Matter Mater. Phys.* **1986**, *33*, 7069−7076.

(25) Scardera, G.; Puzzer, T.; Conibeer, G.; Green, M. A. Fourier Transform Infrared Spectroscopy of Annealed Silicon-Rich Silicon Nitride Thin Films. *J. Appl. Phys.* **2008**, *104*, 104310.

(26) Kim, D. S.; Lee, Y. H. Room-Temperature Deposition of a-SiC:H Thin Films by Ion-Assisted Plasma-Enhanced CVD. *Thin Solid Films* **1996**, *283*, 109−118.

(27) Besling, W. F. A.; Goossens, A.; Meester, B.; Schoonman, J. Laser-Induced Chemical Vapor Deposition of Nanostructured Silicon Carbonitride Thin Films. *J. Appl. Phys.* **1998**, *83*, 544−553.

(28) Socrates, G. *Infrared and Raman Characteristic Group Frequencies: Tables and Charts*, 3rd ed.; John Wiley & Sons, Ltd, 2004; p 366.

(29) Bustarret, E.; Bensouda, M.; Habrard, M. C.; Bruyère, J. C.; Poulin, S.; Gujrathi, S. C. Configurational Statistics in a-$Si_xN_yH_z$ Alloys: A Quantitative Bonding Analysis. *Phys. Rev. B: Condens. Matter Mater. Phys.* **1988**, *38*, 8171−8184.

(30) Stuart, B. H. *Infrared Spectroscopy: Fundamentals and Applications*; John Wiley & Sons, Ltd, 2004; p 224.

(31) NIST Chemistry WebBook. http://webbook.nist.gov/chemistry/.

(32) Abdelli-Messaci, S.; Kerdja, T.; Bendib, A.; Malek, S. CN Emission Spectroscopy Study of Carbon Plasma in Nitrogen Environment. *Spectrochim. Acta, Part B* **2005**, *60*, 955−959.

(33) Mackus, A. J. M.; Heil, S. B. S.; Langereis, E.; Knoops, H. C. M.; van de Sanden, M. C. M.; Kessels, W. M. M. Optical Emission Spectroscopy As a Tool for Studying, Optimizing, and Monitoring Plasma-Assisted Atomic Layer Deposition Processes. *J. Vac. Sci. Technol., A* **2010**, *28*, 77−87.

(34) Laidig, W. D.; Yamaguchi, Y.; Schaefer, H. F. Where to Look for the Electronic Spectrum of Hydrogen Isocyanide, HNC. *J. Chem. Phys.* **1984**, *80*, 3069−3072.

(35) Bu, Y.; Ma, L.; Lin, M. C. Interaction of HCN/DCN with Si(100)-2 × 1. *J. Phys. Chem.* **1993**, *97*, 7081−7087.

(36) Bu, Y.; Ma, L.; Lin, M. C. Interaction of HCN (DCN) with Si(111)-7 × 7 Studied with HREELS, UPS, and XPS. *J. Phys. Chem.* **1993**, *97*, 11797−11801.

(37) Di Mundo, R.; D'Agostino, R.; Fracassi, F.; Palumbo, F. A Novel Organosilicon Source for Low Temperature Plasma Deposition of Silicon Nitride-Like Thin Films. *Plasma Processes Polym.* **2005**, *2*, 612−617.

(38) Tiznado, H.; Bouman, M.; Kang, B. C.; Lee, I.; Zaera, F. Mechanistic Details of Atomic Layer Deposition (ALD) Processes for Metal Nitride Film Growth. *J. Mol. Catal. A: Chem.* **2008**, *281*, 35−43.

(39) Bacalzo-Gladden, F.; Lu, X.; Lin, M. C. Adsorption, Isomerization, and Decomposition of HCN on Si(100)2 × 1: A Computational Study with a Double-Dimer Cluster Model. *J. Phys. Chem. B* **2001**, *105*, 4368−4373.